A NEW HIGH-IRRADIATION IGNITION TEST AND DIAGNOSIS METHOD OF SOLID COMBUSTIBLES

Liu LIU[1,2], Yu-shi WEN[2], Dan WANG[3], Hong YANG[2], Xiao-gan DAI[2], Chang-gen FENG[1], Qiang GAN[1*], Yang ZHOU[2*]

1. State Key Laboratory of Explosion Science and Technology, Beijing Institute of Technology, Beijing, China;

2. Institute of Chemical Materials, China Academy of Engineering Physics, Mianyang, China;

3. Institute of Applied Electronics, China Academy of Engineering Physics, Mianyang, China

[*] Corresponding author; E-mail: zhouy@caep.cn; ganqiang@bit.edu.cn;

This study proposes a new high-irradiation ignition test method for studying the pyrolysis and ignition of solid combustibles under extreme scenarios (> 0.1 MW·m^{-2}). The irradiation system that generates a 10-cm octagonal spot of dynamic irradiation with a peak flux of 1.25 MW·m^{-2} and 95% uniformity, and a chamber with well-controlled ambient conditions and advanced diagnostics coupled with a multi-physical parameter measurement system. A verification test was conducted on corrugated cardboard using the proposed test method, resulting in high-quality outcomes with lower coefficients of variation compared to previous test methods. This improved approach provides a better procedure for testing and understanding the ignition threshold of combustible materials and laying the foundation for the development of advanced models of material pyrolysis and ignition processes under high irradiation.

Key words*: High heat flux; irradiation; pyrolysis; ignition; fire*

1. Introduction

The pyrolysis and ignition thresholds of solid combustibles are key parameters for both the fire assessment and protection, showing important application prospects in the military, national defence, industry, and other fields. While traditional fire tests have provided insight into pyrolysis and ignition characteristics under medium levels of irradiation flux of kW·m^{-2} [1,2], extreme scenarios including strong explosions [3, 4], directed-energy weapons [5], propellant fires [6], arcs [7] and meteorite impacts [8], can reach irradiation levels of MW·m^{-2}. Understanding the response of solid combustibles under high dynamic irradiation is challenging due to method and equipment limitations. Milosavljevic *et al.* [9] reported that the chemical reaction rate of the material under high irradiation is extremely sensitive to the heating rate. Moreover, high irradiation alters the ignition mechanism from diffusion-controlled to ablation-controlled, rendering traditional models and empirical approaches inapplicable [10]. Therefore, a high-irradiation ignition test and diagnosis method is necessary to enhance our comprehension of pyrolysis and ignition characteristics under such high irradiations, thereby mitigating fire hazards.

Pioneer experiments since the 1950s have provided insight into ignition mechanisms under small-scale high irradiations. Martin *et al.* [10] established the framework for such tests, with a peak heat flux of 1 $MW \cdot m^{-2}$ and a 2.3 cm spot size. While Lopatina *et al.* [11] used xenon lamps to generate high irradiation with 4 $MW \cdot m^{-2}$ and an 87% uniformity in light intensity. Other researchers proposed alternative methods, including Kashiwagi *et al*. investigated the orientation effect of sample orientation on ignition of oak and PMMA using a 2.5 cm Gaussian CO_2 laser spot with fluxes of 0.2 MW/m^2 [12, 13], and the investigation was further advanced via numerical calculations [14] and experiments [15], with a smaller Gaussian spot size of 0.5 cm but a higher central flux up to 2.05 MW/m^2. Additionally, Nakamura *et al.* reported slightly a higher flux of 0.213 MW/m^2 with 0.77 cm spot size in experimental studies for space environments [16]. Huang *et al.* [17] focused sunlight to a 0.15 cm spot with fluxes of 0.78 $MW \cdot m^{-2}$ to investigate the smoldering ignition of tissue paper. These methods have advanced our understanding of material behavior under high irradiations. However, small-scale tests may overestimate the ignition threshold due to large convective heat losses and gas dilution effects [18], while spot sizes of 0.5-5 cm are insufficient for anisotropic fuels with characteristic lengths of centimeters, such as natural wood sample with centimeter-level alternating grains and anisotropic properties.

Recently, Brown has utilized concentrated solar energy to generate irradiation spots of 5 cm and 1 m diameters. Although the peak irradiation can reach 1 $MW \cdot m^{-2}$, the distribution of the irradiation is Gaussian, indicating relatively poor uniformity. However, the tests conducted in open-air conditions led to uncertainties in ignition threshold due to uncontrollable ambient conditions and difficulties in identifying critical images from optical cameras [19]. Thus, there is a knowledge gap that needs to be addressed by developing advanced test methods to accurately investigate ignition using high-quality irradiation and repeatable conditions.

To optimize the spatiotemporal distribution of irradiation, reduce the uncertainties from the uncontrollable ambient conditions, and to obtain higher accuracy results in more aspects, a new high-irradiation ignition test and diagnosis method with the peak flux of 1.25 $MW \cdot m^{-2}$ and the spot size of 10-cm were proposed here. A high-power laser was applied as the radiation source, and the intermediate-scale irradiation intensity was homogenized. The test chamber with controllable ambient conditions was incorporated with an integrated diagnostics system capable of measuring multiple parameters. The verification test on corrugated cardboard was conducted using dynamic high irradiation. Our work will advance the development and verification of advanced pyrolysis and ignition calculation models.

2. Systems and method

2.1. High heat flux irradiation system

2.1.1 Irradiation system design and structure

We established a high-fidelity irradiation system with a self-developed solid-state laser, which has high electro-optical conversion efficiency over 55%, higher than fiber (~ 30%) and YAG (~ 15%) based ones. In addition, the peak wavelength and its full width at half maximum were 935 nm and 5 nm respectively, with relative spectral power following Lorentzian distributions. A computer program was developed to control both the power supply the laser and the trigger. The compact irradiation system (**Figure 1**) includes a stacked laser diode bar array module (>22 kW), cylindrical lenses, and

an octagonal dielectric waveguide for beam homogenization. The waveguide structure was fully enclosed and water-cooled to reduce thermal effects and exclude external pollutants and light pollution. The output from the beam-homogenizing system was imaged, expanded, and ultimately formed a uniform high-irradiation spot at a predetermined position of 2 m on the sample surface.

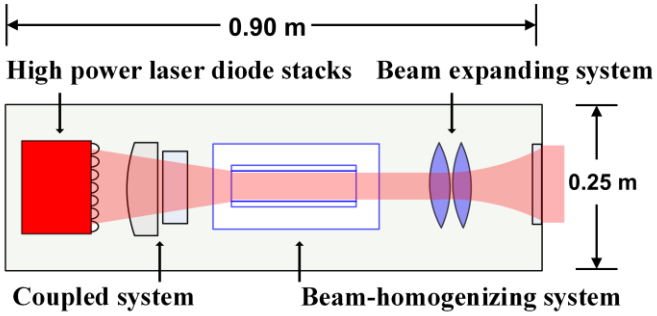

Fig. 1. Schematic diagram of the high irradiation system

2.1.2 High irradiation characterization

The light path shown in **Figure 2** was constructed to characterize the high-irradiation spot in terms of shape, size, uniformity, intensity, and temporal profile. A laser beam profiler (36×36 mm), power meter (500w), Si photodiode (400-1700 nm), a standard diffuse reflector, oscilloscope, and two wedged mirrors were used to capture and measure these parameters. Results showed that the irradiation system formed a regular octagonal spot with an inscribed circle diameter of 10 cm at the specified sample location, exhibiting 95% uniformity (**Figure 3**) and a peak irradiation of 1.25 $MW \cdot m^{-2}$.

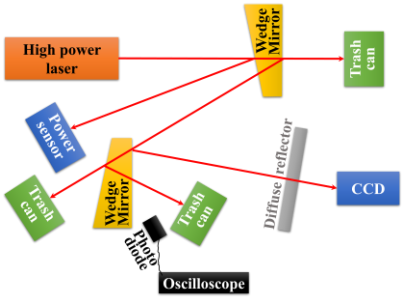

Fig. 2. Schematic diagram of the light path for the irradiation parameters measurement

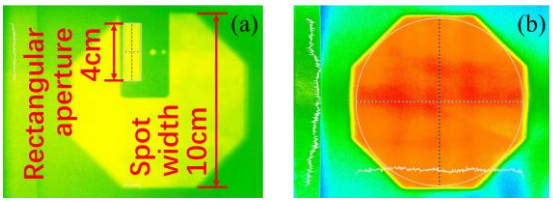

Fig. 3. Spatial profile of the irradiated spot: (a) shape and size (b) irradiation uniformity

2.1.3 Dynamic waveform design

To simulate the complex irradiation in extreme scenarios such as strong explosion [3], precise dynamic irradiation is required. To fit the temporal profile of the strong explosion irradiance, a multi-level ladder waveform was designed, and a program-editing software was adopted. The generated fitting irradiance and fluence curves in red showed excellent stability over 95%, with a relative error of about 6% when compared to the measured strong explosion curves in black, as shown in **Figure 4**.

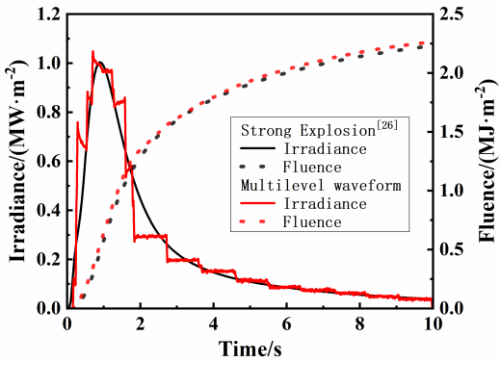

Fig. 4. Comparison of temporal profiles of explosion irradiance and fluence between literature (black) and fitting (red) results.

2.2. Multi-function test chamber system

A semi-closed multi-function test chamber, shaped like an octagonal prism with 2m width and height (with schematic diagram in **Figure 5**.), was constructed to maintain accurate and controllable ambient conditions during testing. The chamber has several air inlets and an exhaust pipe with a filter to facilitate emission of gas products and smoke after tests. Optical observations were made through quartz glass windows and infrared imagery through sapphire glass window (over 90% transmission in 2-4.5 μm). The laser beam passed through a coated glass window and vertically irradiated the sample in the geometric center of the chamber. Temperature control accuracy of 1℃ and humidity control accuracy of 5% were achieved by atmosphere monitoring and cntrolling.

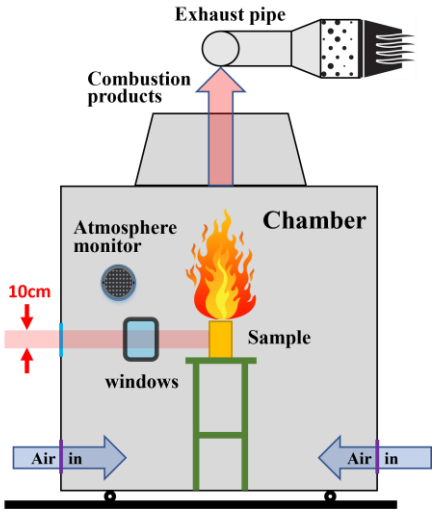

Fig. 5. Schematic diagram of the multi-function test chamber under irradiation.

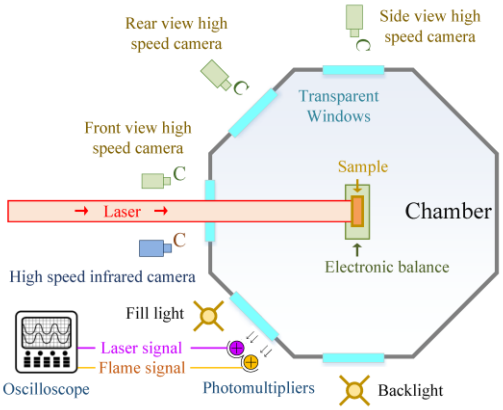

Fig. 6. A top-view layout of the experimental setup.

2.3. Diagnostics

To monitor the pyrolysis and ignition characteristics, a diagnostic system was established to measure various physical parameters. This system includes high-speed optical photography and infrared thermal imaging, as well as in-situ measurement of dynamic mass loss, as illustrated in

Figure 6. These devices were triggered synchronously by a computer program that also controlled the irradiation system. More information on the equipment can be found below.

2.3.1 High-speed optical photography

Accurately measuring key parameters such as pyrolysis and ignition delay times and flame sustainability is crucial. However, the time to trigger pyrolysis and ignition is only 0.1-10 s under high irradiation, leading to possible obscure of the framelet (the sign of ignition) by moving opaque pyrolysis gases, and consequently misjudgment of delay time based on a single view [18]. To address this, three high-speed optical cameras (100 fps) were employed to synchronously record the test process from rear-front-side views, while deploying filters and LED to avoid interference and overexposure. Backlighting was used to capture gas emission from the sample surface for pyrolysis initiation determination.

2.3.2 High-speed infrared imagery

Quintiere [20] approximated the temperature of the pyrolysis gases as the sample surface temperature. Therefore, a high-speed infrared camera (100 fps) was used to record the infrared spectral response of the sample surface. The camera had a 50 mm lens and a spectral band in the 3-5 μm, calibrated from 133 ℃ to 1500 ℃, along with a sapphire glass. The temperature of the sample's surface was calculated based on its emissivity, target distance, and other parameters using post-processing software. The distance between the infrared camera and the sample plane was 1.67 m. The chronometer error was less than 0.01 s, and the temperature error was -1.88 ℃, validated with a blackbody at 597.8 ℃.

2.3.3 High time resolution electronic balance system

The mass loss of solid combustibles is a reliable indicator of the heat released during pyrolysis, ignition, and combustion. The concentration of pyrolysis gases is also reflected in mass loss. Additionally, the ignition delay time could be linked to a critical mass flux leaving the exposed sample surface. Therefore, it is necessary to measure the dynamic mass loss of the solid combustibles during testing. For this purpose, a high-precision electronic balance (AXA30002, Asone) with a high-time resolution was used to measure the dynamic mass during tests. The data was transmitted to the computer in real-time through the RS-232 communication interface at a sampling rate of 10 Hz. To prevent damage to the electronic balance, an insulation board was placed on it to isolate the heat from the burning sample.

3. Verification test

3.1. Sample, test conditions and procedures

To verify the reliability and accuracy of the test system, corrugated cardboard, a common combustible in urban areas, was chosen for the verification test. Its properties resemble those of the cellulose used in previous studies [18], enabling a comparison of experimental results. The corrugated cardboard had a sandwich structure with two outer layers and a middle layer of corrugated medium, and measured 10×10×3 cm, with an emissivity of 0.95 [21, 22]. The temporal profile of applied high

dynamic irradiations was shown in **Figure 4**, with peak values 0.40-1.25 MW·m^{-2}. The test was conducted in a windless environment at a temperature of (20±1) ℃ and relative humidity of (60±5)%, with the air inlets and outlet devices closed, and the ambient pressure at (95±1) kPa. The sample was mounted on a frame on the electronic balance.

During the test, the observation continued even the irradiation was ended, to identify if flaming ignition sustains. After the test, the air inlets and outlet devices were opened, and the gas products and the smoke were extracted from the chamber into an exhaust pipe with a filter until the atmosphere including temperature, humidity and proportion of oxygen were all restored. To ensure experimental repeatability, all the tests were repeated three times. The acquired data were further processed to obtain the average value μ, the standard deviation σ, and the coefficient of variation (CV) = σ/μ.

3.2. Test results

3.2.1 Fire phenomena and pyrolysis & ignition delay times

Figure 7 illustrates the fire phenomena of corrugated cardboard under 0.4 MW·m^{-2} dynamic irradiation, arranged from left to right by rear-front-side camera images. The initial frame where the unfiltered laser spot was visible in the rear view determined the zero time. The cardboard underwent a standard evolution process of water evaporation, pyrolysis, flaming ignition, and decay. From **Figure 7 (a–b)**, water evaporation caused a slight color change on the exposed area, and the cardboard began to bend due to thermal stress. As compared from **Figure 7 (b–c)**, pyrolysis led to gas ejection from the exposed area and the corrugated medium holes, forming premixed combustible gases. At the same time, the exposed area was oxidized due to the high temperature, and glowing spots could be observed. Then, as shown in **Figure 7 (d–e), i**gnition of combustible gases caused a strong fire plume and solid residues to crack, bulge and spall. As the dynamic flux gradually reduced to zero, the flame length decreased, but the corrugated cardboard continued to burn until all combustible ingredients were consumed.

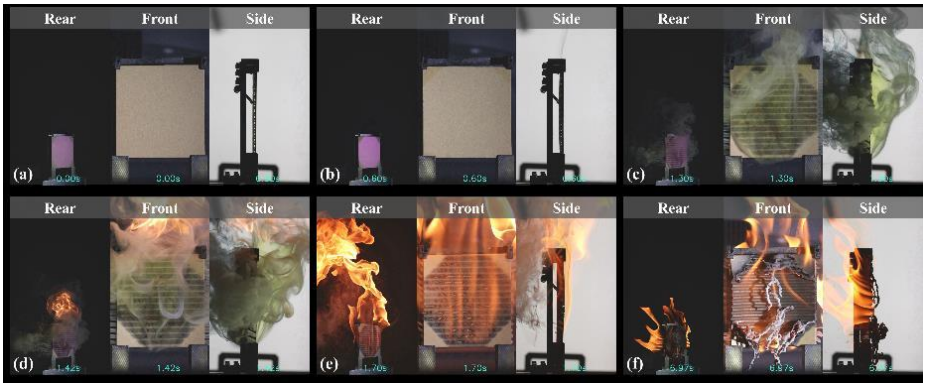

Fig. 7. Fire phenomena of corrugated cardboard under 0.4 MW·m^{-2} dynamic irradiation.

The pyrolysis delay time (t_{pyr}) and ignition delay time (t_{ig}) are determined by observing the emission of translucent smoke and first flame appearance, respectively, as shown in **Figure 7(b) and (d)**. **Figure 8** summarize the results, which show a low CV of less than 18%. The high repeatability of the irradiation system and controlled environmental conditions in the chamber contributed to negligible diagnostic errors. However, the main source of error was the repeatability of the corrugated cardboard.

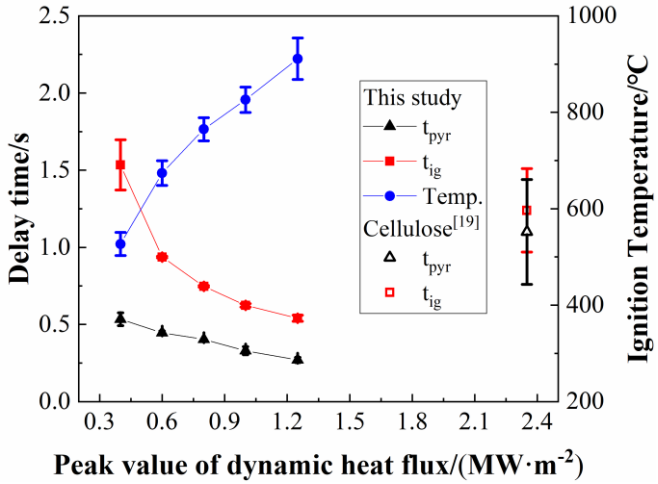

Fig. 8. Threshold map for the corrugated cardboard test.

3.2.2 Irradiated surface temperature

The high-speed infrared camera recorded spatial-temporal temperature distribution on the irradiated area of the corrugated cardboard under high irradiation. **Figure 9** shows the infrared frames under 0.4 MW·m^{-2} condition. These frames correspond to the images moment in **Figure 7**, except for the first frame, which captures the moment when the temperature first exceeds the lower limit of the measurement range (130-1500 ℃).

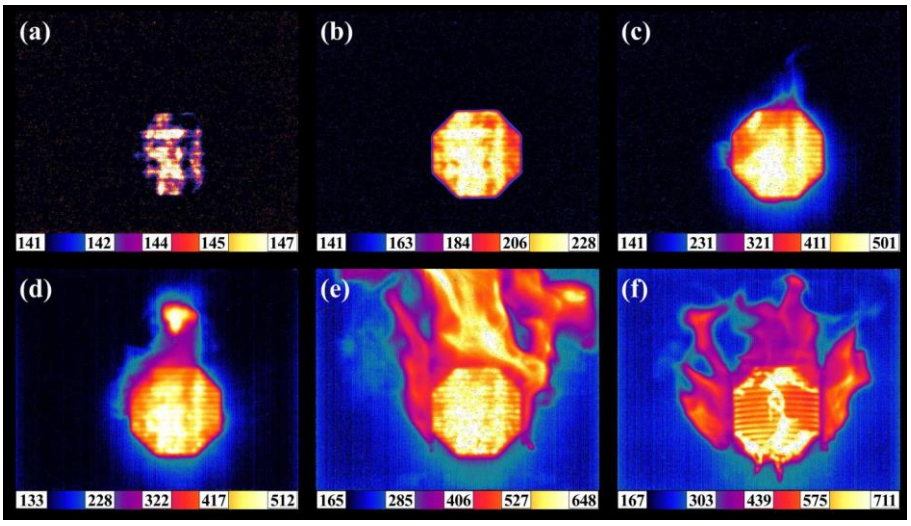

Fig. 9. Infrared images derived from the corrugated cardboard test with (a)-(f) corresponding to time 0.40-0.60-1.30-1.42-1.70-6.97 s, respectively.

This produced curves of the mean temperature profiles of the irradiated area from 30,000 pixels, as displayed in **Figure 10(a)**. The average temperature rise rate was approximately 400 ℃·s^{-1} within the first second. The ignition temperature [20], summarized in **Figure 8**, was determined by calculating the maximum temperatures (Temp.) at the gas phase ignition moment in **Figure 7(d)** and the preceding moment (0.01 s before).

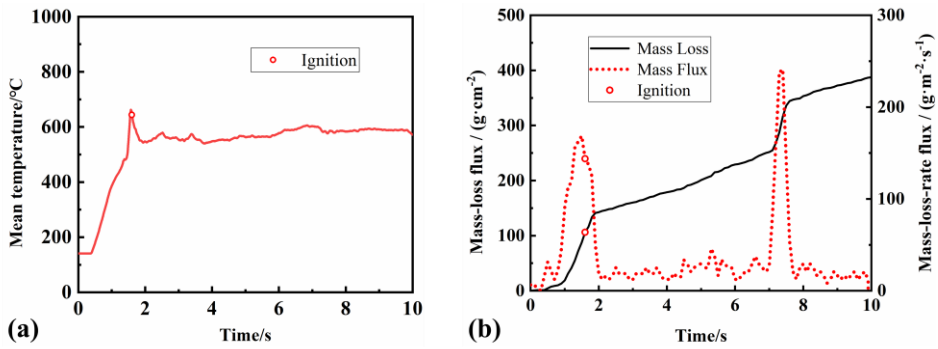

Fig. 10. Mean temperature (a) and mass loss (b) of corrugated cardboard under dynamic 0.4 MW·m^{-2} irradiation over time.

3.2.3 Dynamic mass loss curve

The electronic balance system recorded the dynamic mass loss curve of the corrugated cardboard under 0.4 MW·m^{-2} dynamic irradiation (**Figure 10**(b)). The time resolution was 0.1 ms, which allowed for a high temporal resolution to effectively track the continuous and rapid change process of the mass. This data is crucial in understanding the relationship between the mass-loss rate over time and studying the dynamic radiation attenuation effects of the pyrolysis volatiles on ignition.

3.2.4 General conclusion

The irradiation experiments were conducted under dynamic fluxes ranging 0.40-1.25 MW·m^{-2} at 10-cm scale with 95% uniformity. The material responses, delay times, surface temperature and mass flux were recorded with high-speed optical and infrared cameras, and high time resolution balance. The multi-function test chamber system maintained controlled ambient conditions, ensuring the reliability of the collected data. This new high-irradiation ignition test method demonstrates its potential for evaluating the pyrolysis and ignition characteristics of solid combustibles under intermediate-scale high irradiations.

4. Discussion

4.1. Ignition mechanism of corrugated cardboard under high heat flux

The flaming ignition occurred in the pyrolysis plume above the irradiation region, as shown in **Figure 7** (c~d). Flaming ignition requires the fuel-oxygen ratio to be within flammable limits [23] and the temperature was sufficiently high to initiate and accelerate gas phase chemical reactions [13]. While the emitted gas was assumed to have the same temperature as the irradiated area [20], which

was measured 580-640℃ before ignition. It is inferred that the plume was heated to a temperature high enough for auto-ignition before being transported out of the radiation region. However, the local fuel gas concentration in front of the irradiated surface was too rich to be ignited. This mechanism indicates that mixing time play an important role in high heat flux ignition of solid combustibles.

The absorption of radiation by pyrolysis gases are recognized a primary cause of autoignition [24]. However, when radiation is directed downwards onto a vertical orientation sample, the attenuation of irradiation is only 10-20% [13], whereas it is 75-80% in horizontal orientation [12]. Unlike previous experiments with CO_2 lasers, the infrared irradiation used in this study has a shorter wavelength. This could result in a higher scattering/absorption ratio of pyrolysis gases. Therefore, the absorption of radiation by a thinner layer of pyrolysis gases (**Figure 7**) in this study may be relatively insignificant.

4.2. High heat flux irradiation loading technique.

Table 1 compares the high irradiation loading technology reported by Sandia National Laboratory (SNL), Tomsk State University (TSU), and this work. Despite using a lower irradiation level (one third to half of SNL [18] and TSU [25]), this work achieved better performance due to a larger spot size and higher uniformity. The spot diameter in this work is twice that of SNL and five times that of TSU, minimizing scale effects of convective heat losses, heat diffusion, and material heterogeneity. The 95% spot uniformity surpasses SNL's Gaussian distribution [26] and TSU's 87% [27], making it closer to real scenarios. Additionally, the temporal profile in this work is more flexible and can accommodate complex profiles of extreme scenarios, such as strong explosions.

Table 1. Comparison of the different high irradiation loading technologies.

	Peak flux /($MW \cdot m^{-2}$)	Spot shape and size/cm	Uniformity	Exposure profile
Sandia National Laboratory [18, 28]	2.3	Circle 5	Gaussian distribution	Asymmetric trapezoidal wave
Tomsk State University [25, 27]	4	Circle 2	87%	Trapezoidal wave
This work	1.25	Octagon 10	95%	Any complex profiles can be generated

4.3. Test environment and loading condition of the control technique

The SNL's field test using sunlight encountered numerous uncertainties that were difficult to measure [18]. The irradiation was heavily influenced by factors such as reflective panels, sunlight angle, and weather conditions, and testing was only feasible at noon on a sunny day without strong winds, while the irradiation calibrations are also needed before and after each test, leading to complex procedures and reduced operational efficiency. Additionally, there were also uncontrollable environmental variables, including wind speed and direction, with CV up to 60% and 30%, respectively. Therefore, airflow led to dilution of pyrolysis gas, resulting in random ignition times [29], and humidity affected the ignition delay time by altering the material's moisture content and thermal conductivity [30]. In contrast, in this work, irradiation tests are conducted in a semi-closed multi-functional chamber that allows for control of the ambient temperature, humidity, wind direction, and speed, irrespective of weather conditions. With the stable irradiation performance generated by laser,

there is no frequent need to calibrate the irradiation parameters, resulting in improved operational efficiency.

4.4. Diagnostics for key parameters of the irradiation effects

In SNL's tests, the intense scattering of high solar irradiation led to overexposure of optical cameras and hindered the identification of crucial phenomena [26]. while adding more cameras with filters provided limited improvement [28]. Mass measurements in these tests only recorded the total mass loss before and after the experiment [18]. In contrast, this study employed selective filtering of near-infrared irradiation and supplementary LED light to provide clear observation of fuel surface and plume boundary **(Figure 6)**. Moreover, calibrated surface temperature data from the high-speed infrared camera was used to evaluate the behavior of solid combustibles under high irradiation.

The surface temperature is important in evaluating solid combustible behavior. **Figure 7(c-e)** shows the plume thickness increases with height, which matches the description of flaming ignition [31]. The effect of the plume on infrared thermometry could be negligible in this study, with only a minimal difference between the upper and lower halves of the exposed area, based on further data analysis. This is because the particulates in pyrolysis aerosols of carbonous materials are 30 nm-2 μm [32, 33], which are smaller enough to allow 3-5 μm infrared radiation to pass through them without significant scatter based on the diffraction theory, as confirmed in **Figure 10(a-d)**. The initial flame in Figure **10(d)** was visible due to the emission of energy at 4.3 μm from hot CO_2 [34], which is within the infrared camera's spectral range. Both pyrolysis and flame plumes were not optically thick enough to cause significant radiation absorption or emission radiation since their thickness did not exceed 0.05 m in this study.

Improved acquisition programs led to a time resolution of 0.1 s for measuring mass loss, which allowed for the calculation of critical mass loss rate. Optical images were needed to identify spalling solid residues to avoid inaccurate mass flux predictions. In summary, the use of diagnostics integrated with multi-physical parameter measurement is essential for understanding the phenomenon and validating model predictions.

4.5. Comparison of the coefficient of variation of key result data

Brown *et al*. [19] found the CV of cellulose pyrolysis and ignition delay time to be 30.83% and 20.70%, respectively. However, the CVs of corrugated cardboard (also a cellulose material) tested in this study were lower, ranging from 1.43% to 17.87% and from 0.77% to 10.60%, respectively **(Figure 8)**. These results demonstrate better repeatability and accuracy than those reported by SNL, indicating that the proposed method offers superior control of ambient conditions and improved diagnostics through multi-parameter data acquisition. Thus, the proposed method provides more reliable results for subsequent research on fire behavior and ignition threshold.

5. Conclusions

This work presents a new method for high-irradiation ignition testing to characterize the pyrolysis and ignition behavior of solid combustibles under extreme heat flux. The main findings are as follows: (1) A new high-irradiation system with a peak heat flux of 1.25 $MW \cdot m^{-2}$, a diameter of 10 cm and a uniformity of up to 95% was developed, featuring a multi-level ladder waveform that

emulates the dynamic temporal profile of irradiance. (2) A multi-functional test chamber system was built to accurately control environmental variables, while multi-physical parameter diagnostics were employed to measure the pyrolysis and ignition delay time, temporal-spatial temperature distribution, and mass loss over time of corrugated cardboard. (3) The proposed method shows better performance than similar test methods in terms of high-irradiation system quality, controlled ambient conditions, and accurate parameters measurements, with lower coefficients of variation for delay times. This advanced method provides reliable and accurate results that can be used to develop and verify pyrolysis and ignition calculation models for solid combustibles under high heat flux conditions.

Acknowledgements

We would like to thank Dr. WANG Xing from CAEP Software Center for High-Performance Numerical Simulation, for insightful discussions on this project as well as for providing helpful comments during manuscript revision.

References

[1] Ma Y., *et al*., Effect of sample thickness on concurrent steady spread behavior of floor- and ceiling flames, *Combust Flame*, *233* (2021), pp. 111600. https://doi.org/10.1016/j.combustflame.2021.111600

[2] Lin S., *et al*., Piloted Ignition of Cylindrical Wildland Fuels Under Irradiation, *Frontiers in Mechanical Engineering*, *5* (2019), pp. https://doi.org/10.3389/fmech.2019.00054

[3] Tian Z., *et al*., Numerical Investigation of Early Fireball of Strong Explosion for Different Altitudes[J], *Acta Armamentarii*, 30 (2009), 8, pp. 1078-1083.

[4] Glasstone S., *et al*. *The effects of nuclear weapons*, Department of Defense, Washington DC, USA, 1977

[5] Zhang Y. X., *et al*., Damage to aircraft composite structures caused by directed energy system: A literature review, *Defence Technology*, *17* (2021), 4, pp. 1269-1288. https://doi.org/10.1016/j.dt.2020.08.008

[6] White R. B., *et al*., Effect of aluminum on heat flux from a simulated rocket propellant flame, *J Propul Power*, *23* (2007), 6, pp. 1255-1262

[7] Cressault Y., *et al*., Properties of air − aluminum thermal plasmas, *Journal of Physics D: Applied Physics*, *45* (2012), 26, pp. 265202

[8] Svetsov V., *et al*., Thermal radiation from impact plumes, *Meteorit Planet Sci*, *54* (2019), 1, pp. 126-141. https://doi.org/10.1111/maps.13200

[9] Milosavljevic I., *et al*., Cellulose Thermal Decomposition Kinetics: Global Mass Loss Kinetics, *Ind Eng Chem Res*, *34* (1995), 4, pp. 1081-1091. https://doi.org/10.1021/ie00043a009

[10] Martin S., Diffusion-controlled ignition of cellulosic materials by intense radiant energy, *Symposium on Combustion*, *10* (1965), 1, pp. 877-896. https://doi.org/10.1016/S0082-0784(65)80232-6

[11] Lopatina G. G., *et al.*, *"Opticheskie Pechi" (Optical Furnaces)*, Izd. Metallurgiya, Moscow, 1969.

[12] Kashiwagi T., Experimental observation of radiative ignition mechanisms, *Combust Flame*, *34* (1979), pp. 231-244. https://doi.org/10.1016/0010-2180(79)90098-1

[13] Kashiwagi T., Effects of sample orientation on radiative ignition, *Combust Flame*, *44* (1982), 1, pp. 223-245. https://doi.org/10.1016/0010-2180(82)90075-X

[14] Nakamura Y., *et al.*, Effects of sample orientation on nonpiloted ignition of thin poly(methyl methacrylate) sheet by a laser: 1. Theoretical prediction, *Combust Flame*, *141* (2005), 1, pp. 149-169. https://doi.org/10.1016/j.combustflame.2004.12.014

[15] Gotoda H., *et al.*, Effects of sample orientation on nonpiloted ignition of thin poly(methyl methacrylate) sheets by a laser: 2. Experimental results, *Combust Flame*, *145* (2006), 4, pp. 820-835. https://doi.org/10.1016/j.combustflame.2006.01.008

[16] Nakamura Y., *et al.*, Irradiated ignition of solid materials in reduced pressure atmosphere with various oxygen concentrations – for fire safety in space habitats, *Adv Space Res*, *41* (2008), 5, pp. 777-782. https://doi.org/10.1016/j.asr.2007.03.027

[17] Wang S., *et al.*, Smoldering ignition using a concentrated solar irradiation spot, *Fire Safety J*, *129* (2022), pp. 103549. https://doi.org/10.1016/j.firesaf.2022.103549

[18] Brown A. L., *et al.*, Datasets for material ignition from high radiant flux, *Fire Safety J*, *120* (2021), pp. 103131

[19] Engerer J. D., *et al.*, Pyrolysis Under Extreme Heat Flux Characterized by Mass Loss and Three-Dimensional Scans.,*4th Thermal and Fluids Engineering Conference*, Albuquerque,2019,

[20] Quintiere J. G., A theoretical basis for flammability properties, *Fire and Materials: An International Journal*, *30* (2006), 3, pp. 175-214

[21] McKinnon M. B., *et al.*, Development of a pyrolysis model for corrugated cardboard, *Combust Flame*, *160* (2013), 11, pp. 2595-2607. https://doi.org/10.1016/j.combustflame.2013.06.001

[22] Madding R., Finding R-values of stud frame constructed houses with IR thermography, *Proc. InfraMation, 2008* (2008), pp. 261-277

[23] Hurley M. J., *et al.*, *SFPE handbook of fire protection engineering*: Springer. 2015

[24] Blasi C. D., *et al.*, Numerical model of ignition processes of polymeric materials including gas-phase absorption of radiation, *Combust Flame*, *83* (1991), 3, pp. 333-344. https://doi.org/10.1016/0010-2180(91)90080-U

[25] Kasymov D., *et al.*, Studying the effect of fire retardant coating on the fire hazard characteristics of wood using infrared thermography, *EPJ Web of Conferences*, *159* (2017), pp. 18. https://doi.org/10.1051/epjconf/201715900018

[26] Brown A., *et al.*, Megafire Initiation from Extreme Incident Radiative Heat Flux., *the Megafire Workshop*, Albuquerque,2019,

[27] Kuznetsov V., *et al*., Ignition of various wood species by radiant energy, *Combustion Explosion and Shock Waves - COMBUST EXPL SHOCK WAVES-ENGL, 47* (2011), pp. 65-69. https://doi.org/10.1134/S0010508211010096

[28] Brown A., *et al*., Diagnostics and Testing to Assess the Behavior of Organic Materials at High Heat Flux., *The 2017 International Association of Fire Safety Science Symposium*, Lund,2016

[29] Lai D. Experimental and Model Study on Pyrolysis and Ignition Temperature of PMMA under Wind Influence, PhD. thesis, University of Science and Technology of China, Hefei, China, 2021.

[30] Gong J., *et al*., Effect of moisture content on thermal decomposition and autoignition of wood under power-law thermal radiation, *Appl Therm Eng*, *179* (2020), pp. 115651

[31] Tewarson A., *SFPE handbook of fire protection engineering*, National Fire Protection Association, Quincy, MA, 2002

[32] Wang X., *et al*., Soot formation during biomass pyrolysis: Effects of temperature, water-leaching, and gas-phase residence time, *J Anal Appl Pyrol*, *134* (2018), pp. 484-494

[33] Li N., *et al*., Characteristics of aerosol formation and emissions during corn stalk pyrolysis, *Energies*, *13* (2020), 22, pp. 5924

[34] Kim W., *et al*., Characterization of spectral radiation intensities from standard test fires for fire detection, *Nist Special Publication Sp*, (2001), pp. 91-106

Submitted: 16.01.2023.
Revised: 25.04.2023.
Accepted: 27.04.2023